JEAS

JOURNAL OF ENGINEERING AND APPLIED SCIENCES

Journal of Engineering and Applied Sciences, Volume 21, Number 1, Dec. 2022, 866 - 875

Influence of Magnetic Properties on the Performance of Dual Stator Electric Machine: Part I

Chukwuemeka C. Awah[1*]
[1]Department of Electrical and Electronic Engineering, Michael Okpara University of Agriculture, Umudike, Nigeria
[*]Corresponding Author's E-mail: awahchukwuemeka@gmail.com

Abstract
The influence of magnetic properties on the output characteristics of a high performance dual stator permanent magnet machine is studied in this work, in order to provide adequate guide for electric machine operators on magnetic material selection. Finite element analysis technique is adopted in the performance evaluation, owing to its high level of prediction accuracy. The investigated machine indices are: flux linkage, induced-voltage and torque characteristics. More so, the considered magnetic properties are the residual flux density and coercive force of the following magnets: Ferrite, Aluminium-Nickel-Cobalt (Alnico), Neodymium alloy (NdFeB), and Samarium-Cobalt (SmCo). It is observed that an electric machine that has NdFeB magnet would outperform others having other magnet types, due to its good residual flux density and potential high energy density. The worst machine performance is observed in the machine that has ferrite magnetic material. The obtained peak value of induced-voltage from the ferrite, alnico, SmCo and NdFeB magnets is: 2.35 V, 2.67 V, 5.86 V and 6.12 V, respectively with resultant average torque of 1.35 Nm, 1.44 Nm, 3.07 Nm and 3.30 Nm, respectively, at rated current condition.

Keywords: Dual Stator, Electric machine, Induced-voltage, Magnetic properties, and Torque.

1. Introduction

The influence of magnetic material properties on the electromagnetic output of any given electrical machine/device cannot be underestimated. Due to this significant impact, this present study is set to explore these characteristics on both open circuit and on-load conditions of the compared machine topologies. Moreover, the global energy issues have necessitated research towards the use of low-cost and low energy-density non-rare-earth magnets, as alternatives to the rare-earth ones. Hence, detailed review on these set of magnet types is presented in this section for better insight on their various suitable applications.

A comparative analysis between a typical rare-earth magnet i.e. samarium-cobalt magnet (SmCo) and a non-rare-earth magnet i.e. ferrite magnet reveal that the SmCo-made machines could deliver considerable output torque and power compared to the ferrite magnet topology. However, a comparable electromagnetic performance could be achieved between the duo classes of magnet by increasing the number of turns per phase as well as at least doubling the volume of the used non-rare-earth magnet, as detailed in Kim et al (2016). Albeit, with lower saturation withstand competency against the ferrite magnetic machine. It is reconfirmed in Bonthu et al (2017) that the electromagnetic performance of a non-rare-earth magnetic machine could be upgraded to that of rare-earth equivalent, by increasing the permanent magnet material volume of ferrite by over 200%, in addition to its electric loading amplification to over 16%. Therefore, compactness is a major design challenge when dealing with non-rare-earth electric machines for a similar output compared to the rare-earth ones; the amplified electric loading could also pose some saturation problems.

Although, it is well known that rare-earth magnetic machines particularly the ones made with neodymium have improved performance than its non-rare-earth counterparts; it is established that the non-rare-earth magnetic machines could have competitive low cost advantage over the rare-earth magnets; especially the ones made with

alnico magnets in relation to its productivity, coupled with its excellent temperature withstand potential, (Chen et al, 2014). Also, it is claimed in Obata et al, (2013) that ferrite-made permanent magnet machine could deliver comparable efficiency with that of rare-earth magnetic machine; however, with an appropriate manipulation of the machine's effective axial length. More so, research by Krizan and Sudhoff (2013) shows that if a given electric machine is designed and optimized strictly with respect to the peculiarities of the used magnet characteristics, then, it is possible to obtain a non-rare-earth magnetic machine that has a matching performance with that of its rare-earth equivalent; though, with relevant adjustment of its overall mass. Besides, it is established in Yoon and Hwang (2021) that weight reduction of a given permanent magnet material in an electric machine would consistently introduce a percentage of demagnetization factor in the system.

Furthermore, it is demonstrated in Li et al (2018) that better machine performance could further be realized from ferrite magnetic material in place of rare-earth magnets by adopting the Halbach magnetization strategy, which involves scattered magnetic pole-placement on the rotor, primarily for energy density enhancement of the used ferrite material. Ferrite magnet is usually cheaper than most other magnet types; however, it usually has inferior electromagnetic output compared to others, especially the rare-earth types. Nevertheless, Faiz et al, (2020) shows that competitive output could be obtained from ferrite-made machines relative to their rare-earth equals; though, with higher current density and again increased weight.

Moreover, an integrated electric machine having two classes of magnet is shown to be more promising than the ones that have single type of magnet. Thus, an improved hybrid design of permanent magnet machine containing alnico and neodymium magnets is developed in Xu et al, (2021), for improved machine efficiency. The developed machine in Xu et al, (2021) has good flux-controllability feature with adequate distinct flux routes for each magnet category, in order to enhance the magnetic collaboration between the two magnets, for effective loss reduction coupled with improved demagnetization withstand ability.

Similarly, the right choice of permanent magnet flux linkage of a ferrite-equipped machine is proved to be effective in improving the power factor of the machine, as demonstrated in Bianchi et al, (2015) using analytical techniques. More importantly, direct relationships between the flux density, output torque and magnet flux linkage in the system is proven with mathematical expressions. This approach of power factor enhancement is usually achieved by increasing the volume of the employed ferrite magnetic material. Though, analytical approach to electrical machine analysis generally has drawbacks relating to slight inaccuracy, owing to its vast theoretical assumptions with regard to the existing empirical equations.

Kimiabeigi et al, (2016) proved that the inherent low coercivity and poor output performance of ferrite-made electric machines could be improved by using distributed coil conductors as well as by arranging the magnets in spoke-like manner, in order to boost its airgap flux density and in turn improve the generated output torque. Additionally, the spoke-positions of the magnets could also help to enhance the anti-demagnetization capacity of such machines. However, deployment of distributed windings is naturally associated with high production cost, emanating from the required longer coil conductors compared to the short ones of concentrated winding configuration. Meanwhile, the effectiveness of using spoke-like magnets for both demagnetization withstand potential and torque enhancements is reconfirmed in Yoon and Hwang (2021). In addition, spoke-arranged-magnet type of electric machines could have desirable worth, such as lower total voltage harmonic distortion and reduced cogging torque value, as demonstrated in Faiz et al, (2020).

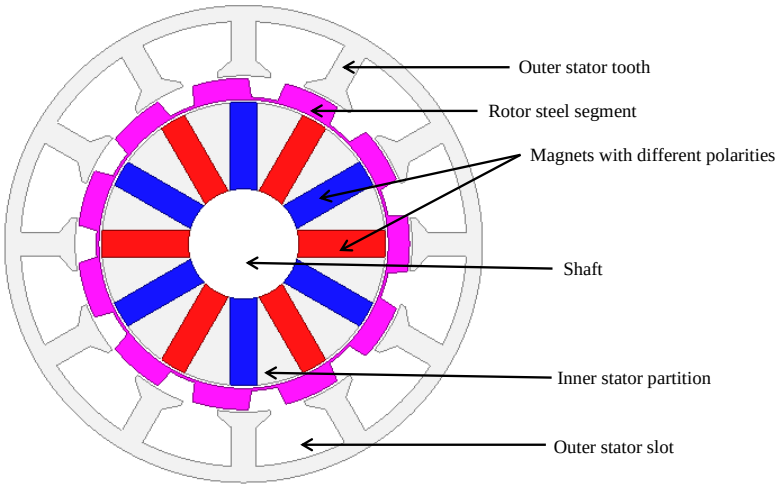

Figure 1: Two-dimensional diagram of the analyzed machine, (Evans and Zhu, 2015)

Above all, the structural orientation of magnets during its manufacturing/magnetization process greatly affects its resulting magnetic properties, particularly its coercive force magnitude, as proved in Xie et al, (2019). Thus, special care should be taken at such early stage in order to yield the required magnetic coercivity and subsequently improved machine performance. Overall, the magnetic influence of both rare-earth and non-rare-earth magnets on the output characteristics of dual stator permanent machine is analyzed and presented in this current study, in order to assist electrical machine designers in choosing the best magnetic materials for different applications. The analyzed machine model is depicted in Figure 1.

2.0 Material and methods

The predicted results in this work are obtained using finite element analysis method. Maxwell-2D version 15.0 simulation software is employed in the calculations. The hardware in this work is a desktop computer with the following specifications: Intel (R) Core i7, 3.40 GHz, 8.00 GB RAM capacity and 64-bit operating system. The used magnet materials are ferrite, Aluminium-Nickel-Cobalt (Alnico), Neodymium alloy (NdFeB), and Samarium-Cobalt (SmCo). It is worth noting that Neodymium (NdFeB) and Samarium-Cobalt magnets are classified as rare-earth magnets while Ferrite and Aluminium-Nickel-Cobalt (Alnico) are non-rare-earth magnets. The stator and rotor core materials are made of silicon steel materials. Note that overall size of the machine is 90 millimeter. Meanwhile, the investigated model has two stators with magnets located in its inner stator, as shown in Figure 1. The predicted flux lines of the machine types are presented in Figure 2. Note that the rare-earth magnets produce more concentrated flux lines than its non-rare-earth equivalents. The total number of turns in the analyzed model is 72 turns per phase with a winding factor of 0.6. Residual flux density of the magnets is: 0.4 Tesla, 1.16 Tesla, 1.05 Tesla and 1.47 Tesla for the ferrite, alnico, SmCo and NdFeB magnetic materials, respectively; it also has corresponding coercive force (coercivities) values of 303 kA/metre, 230 kA/metre, 796 kA/metre and 1063 kA/metre, respectively. Figure 1 is first developed in the project manager section of Maxwell-2D finite element analysis (FEA) software using the existing dimensions and parameters given in Evans and Zhu, (2015). The various parts of the machine are then assigned with relevant material properties from in-built library section of the software. Then, the windings are assigned with relevant number of phase and total number of turns per phase. After which, tiny mesh elements of the parts with special modification on the airgap areas are created for enhanced accuracy; before running the simulation model over a specified electric period. It is worth noting that the automatically-generated finite element results are produced in tabular form over the specified simulation time, before subjecting it to further post-processing in graphical forms.

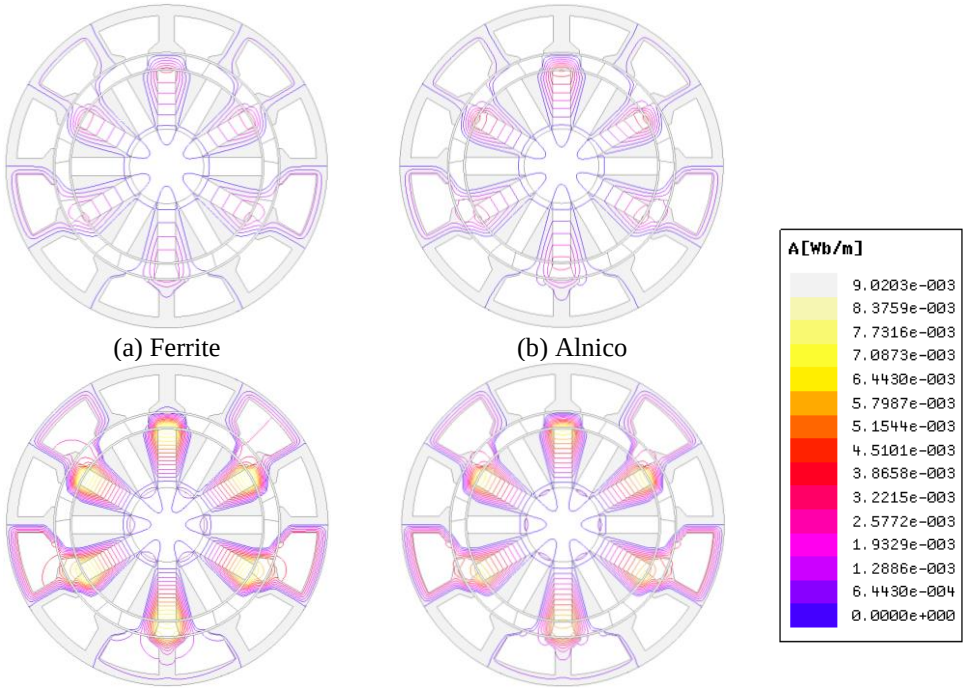

(a) Ferrite (b) Alnico

(c) NdFeB (d) SmCo

Figure 2: Flux outlines on open circuit

The output torque of a given three-phase electrical machine is given in equation 1.

$$T = \frac{E_A I_A + E_B I_B + E_C I_C}{\omega} \quad (1)$$

where: E_A, E_B and E_C are the induced phase voltages, I_A, I_B and I_C are the corresponding supplied phase currents, and ω is the rotor angular velocity.

Similarly, the operating frequency, f (Hertz) of the analyzed permanent magnet machine has a direct proportionality with its number of poles, as evidenced in equation 2. More so, it is established that the induced voltage waveforms of the analyzed machine category would possess symmetrical outline if and only if equation 3 is satisfied, as verified in Chen and Zhu, (2010). Note that the number of stator and rotor poles of the investigated machine model in this study is 12 and 11, respectively, as equally shown in Figure 1.

$$f = \frac{P_r \omega_r}{60} \quad (2)$$

where: P_r is the rotor pole number, and ω_r is the rotor speed (rev/min).

$$\frac{P_s}{HCF(P_s \text{ and } P_r)} = \text{even number} \quad (3)$$

where: P_s and P_r are the stator and rotor pole number, and HCF is the highest common factor between the pole numbers (Chen and Zhu, 2010).

3.0 Results and Discussions

In this section, the obtained finite element results are presented in graphical outlines for ease of assessment of the magnitudes and shapes of generated waveforms in one electric revolution. It is worth mentioning that the plotted results are post-processed from the tabulated computer-automatically-generated finite element analysis (FEA) results. The flux linkage of Phase A is shown in Figure 3(a). The highest value of the phase flux linkage is recorded in the machine that has NdFeB, followed by the SmCo machine type. Maximum value of the phase flux linkage in

the respective magnets is: 0.0053 Webers, 0.0057 Webers, 0.0123 Webers and 0.0131 Webers i.e. from Ferrite-, Alnico-, SmCo- and NdFeB-made electric machines, respectively. Note also that the obtained flux linkage waveforms are sinusoidal and symmetrical, which is a good machine quality. More so, the rare-earth magnets show fairly insensitive response in the variation of its flux linkage with the load current as depicted in Figure 3(b), while its non-rare-earth magnets have linear relationship between the above mentioned two parameters.

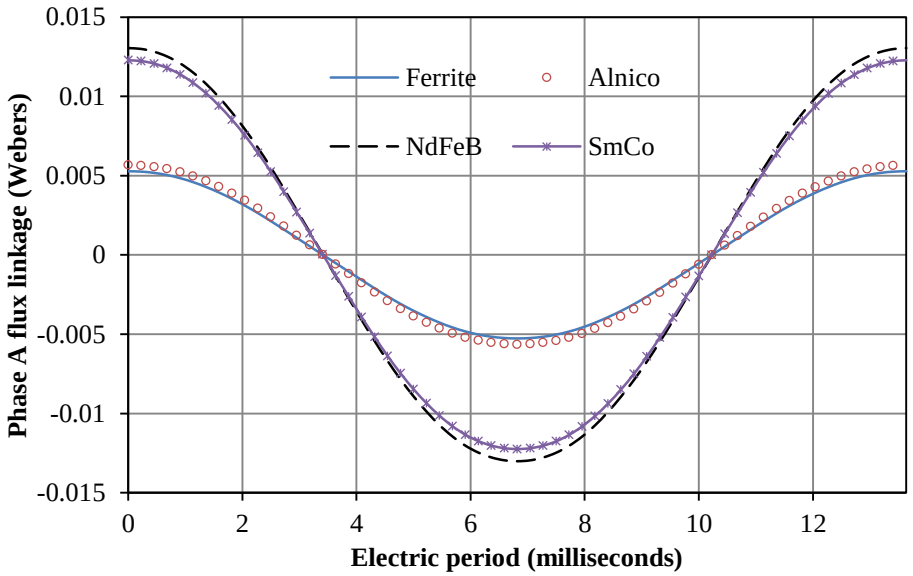

(a) Phase flux linkage versus time

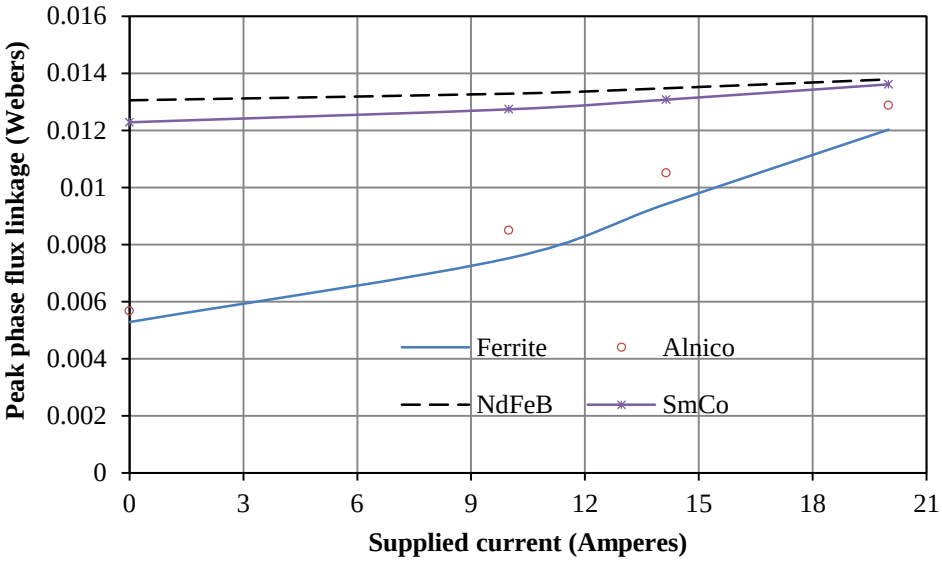

(b) Peak flux linkage versus current

Figure 3: Comparison of phase flux linkage

Further, the induced-voltages of Phase A, Phase B and Phase C of the analyzed machine configurations is displayed in Figure 4. The maximum induced-voltage in the compared four different magnets is: 2.35 V, 2.67 V, 5.86 V and 6.12 V, i.e. from Ferrite, Alnico, SmCo and NdFeB, respectively. Although, the induced-voltages are symmetrical over the simulated period, it is not completely sinusoidal as seen in the plots. This non-sinusoidal voltage waveform weakness is detrimental to the efficient control mechanism of any given electric machine, and it is usually caused by the presence of harmonics in the system. This harmonics effect is reflected in the fast Fourier transform of Figure 5(a), where odd number harmonic components are visible and prevalent. Again, the induced-voltages of rare-earth magnetic machines are less sensitive to the electric loading conditions of the supplied current compared to the non-

rare-earth magnetic ones, as seen from Figure 5(b). Meanwhile, the induced voltages of non-rare-earth magnet have direction proportionality with applied current; nevertheless, with lesser amplitudes than the rare-earth magnetic machines, under similar simulation conditions.

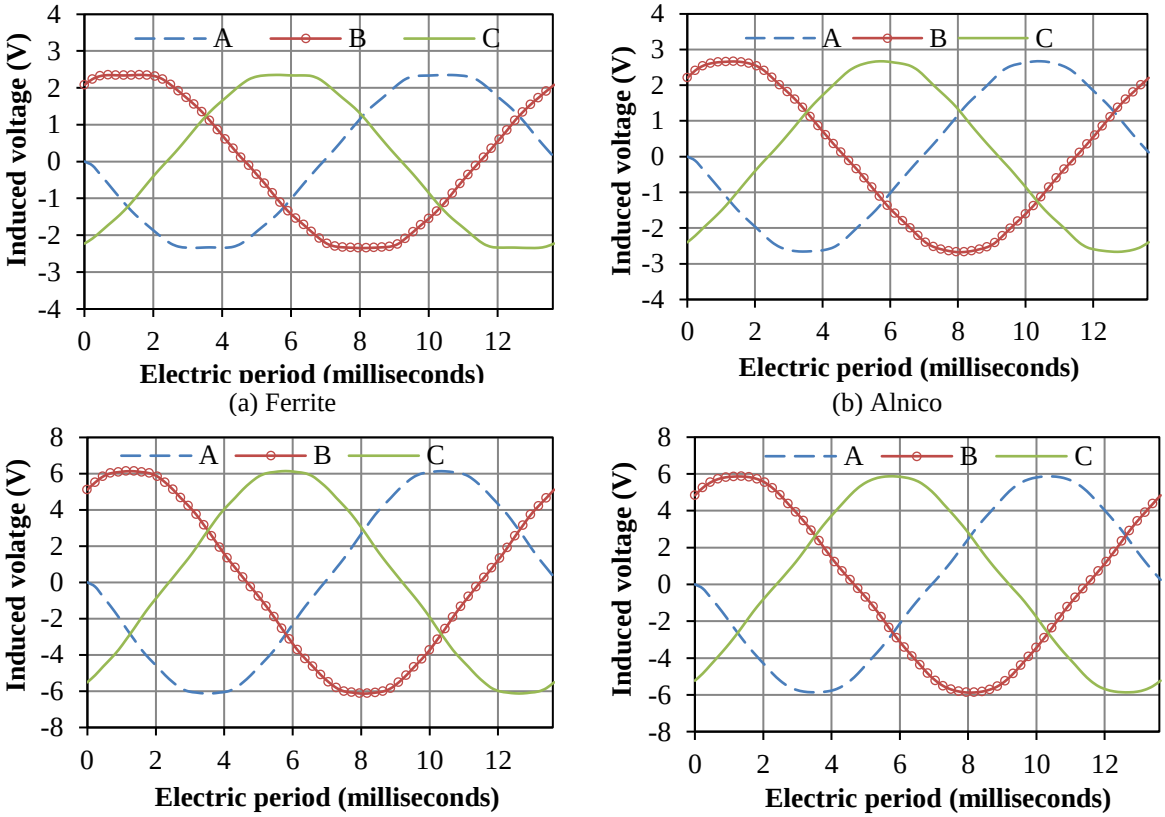

(a) Ferrite (b) Alnico

(c) NdFeB (d) SmCo

Figure 4: Three-phase induced-voltage at 400rpm

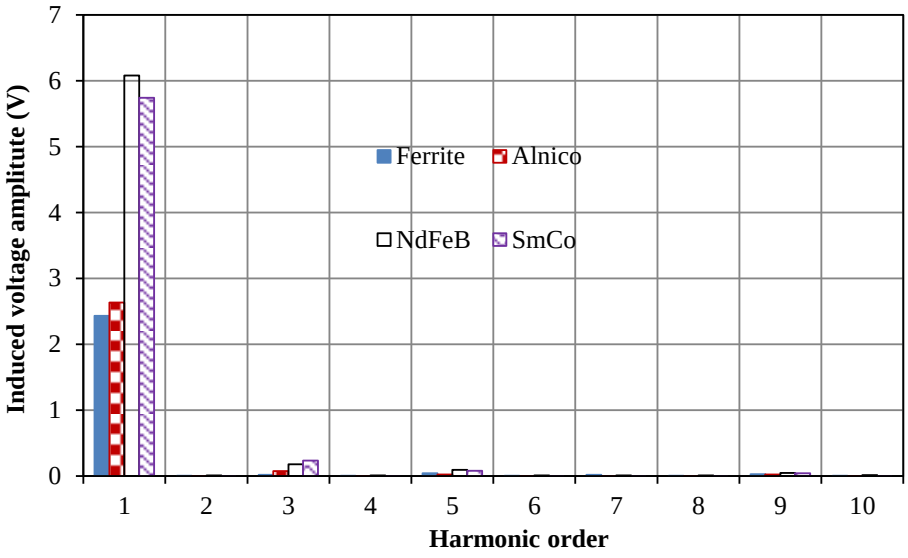

(a) Induced-voltage harmonic order

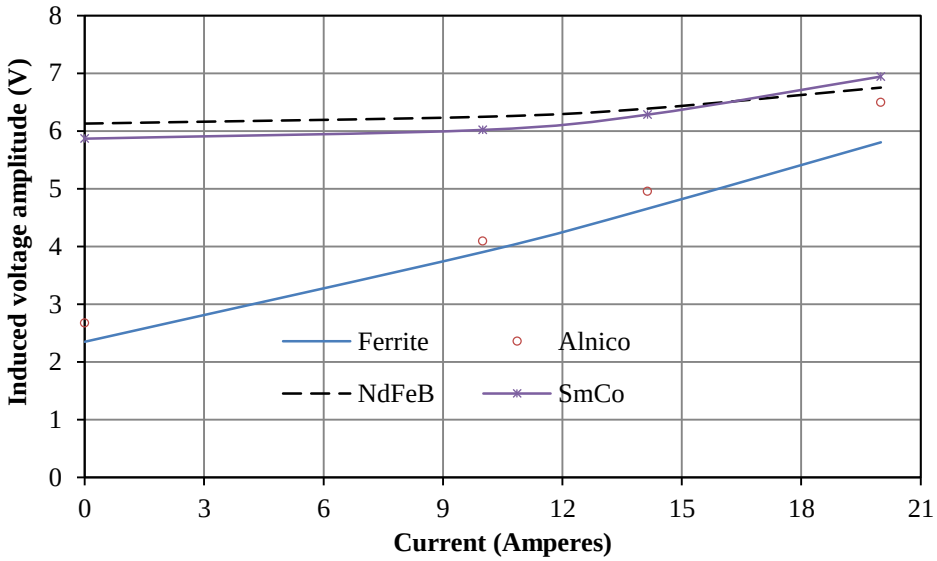

(b) Peak induced-voltage versus current

Figure 5: Comparison of induced-voltage at 400rpm

Furthermore, the electromagnetic output torque of the compared machines is shown in Figure 6. Obviously, the rare-earth magnetic machines exhibit higher torque amplitudes than its non-rare-earth counterparts, owing to its higher residual flux density/magnetic remenance. The finite element predicted output torque of the machines, simulated at 15 Amperes is: 1.35 Nm, 1.44 Nm, 3.07 Nm and 3.30 Nm from Ferrite, Alnico, SmCo and NdFeB magnetic machines, respectively. It is worth noting that the ferrite-equipped machine has the worst electromagnetic torque performance. Note also that the output torque waveforms are evenly distributed over the entire simulation time and hence, over the whole rotor angular positions.

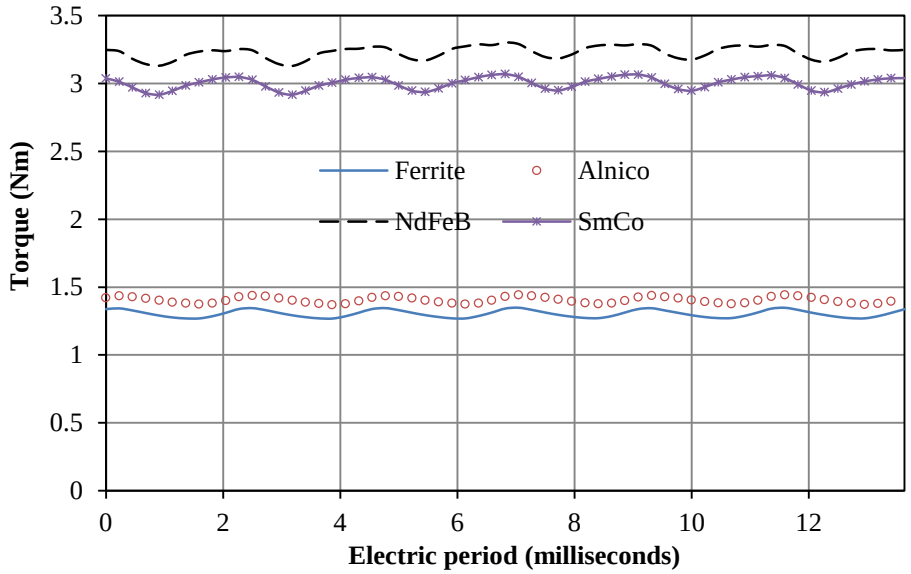

Figure 6: Comparison of electromagnetic torque at 15Amperes

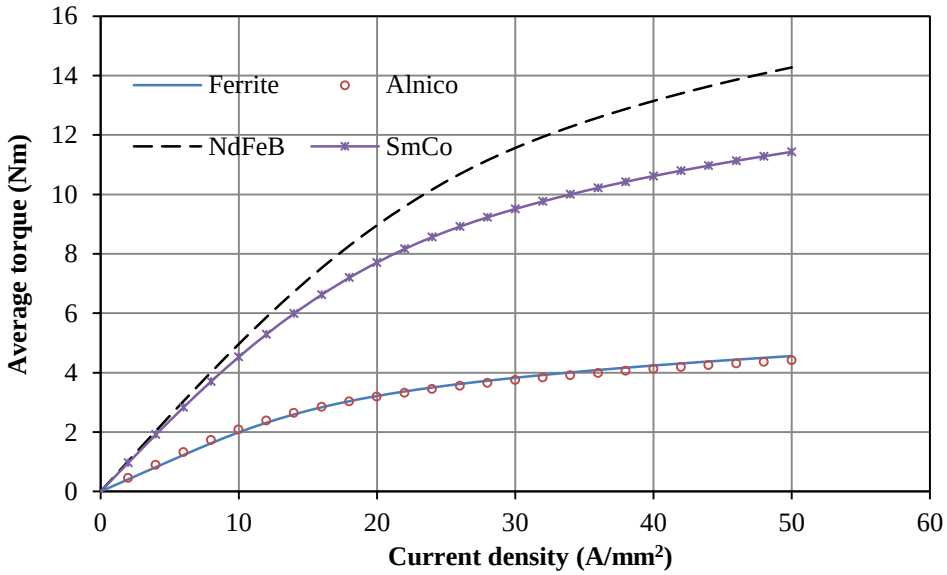

Figure 7: Comparison of average torque

Similarly, the variation of average torque on different current density loadings is depicted in Figure 7. The technical implication of Figure 7 is the magnetic material's ability to withstand overloads. Thus, it is obvious that the machines having rare-earth magnets possess higher overload withstand capacity compared to its non-rare-earth counterparts. It is worth mentioning that the overloading effect on this class of machine is a synergy contribution of both the magnets and armature reaction of the coil/conductors. It should be noted that both ferrite-made and alnico-made investigated machines have similar overload withstand capacity, likely due to its relatively similar and low magnetic coercive forces (coercivities).

Static torque variation of the simulated machine models with the applied current is presented in Figure 8. It is observed that the static torque waveforms are uniformly distributed over the total electric time revolution. More so, magnitudes of the static torque is directly dependent on the applied current i.e. the higher the current, then, the larger its static torque value and vice-versa. Moreover, the electric machine that is furnished with neodymium magnets is the best candidate amongst all the compared machines, in terms of static torque delivery; however, the cost of implementing either neodymium or samarium-cobalt magnets in an electric machine is usually higher than that of ferrite and/or alnico magnets, as mentioned in Awah, (2021).

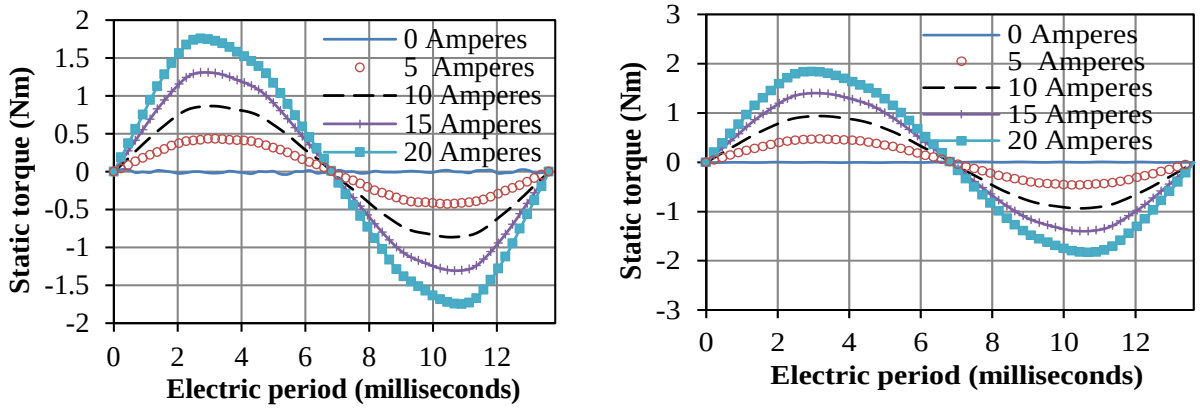

(a) Ferrite (b) Alnico

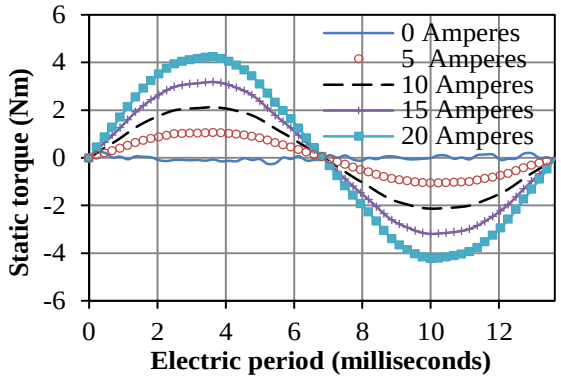

(c) NdFeB

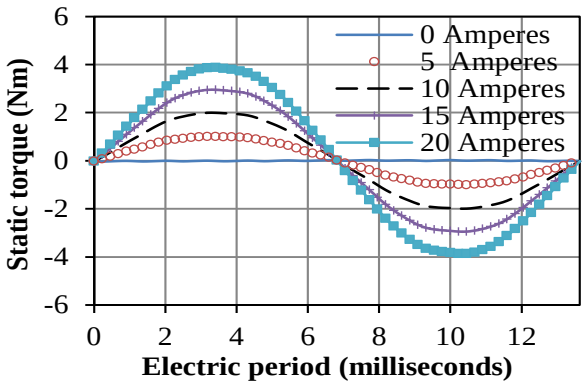

(d) SmCo

Figure 8: Comparison of static torque

4.0. Conclusion

The influence of magnetic properties of different magnets are investigated and presented. It is revealed that the machine having rare-earth magnets such as neodymium and samarium-cobalt has competitive electromagnetic advantage over the other compared magnetic machines like the ones having ferrite and aluminium-nickel-cobalt, owing to its high coercive forces. It is also shown that the machine having ferrite magnets has the poorest electromagnetic performance, followed by the alnico-made machine. Hence, magnetic properties of the employed magnets in an electric machine are great determinants of its electromagnetic performance (s). The investigated machine would be appropriate for high torque direct-drive implementations.

References

Awah, C.C. 2021. Effect of permanent magnet material on the electromagnetic performance of switched-flux permanent magnet machine. Electrical Engineering, 103(3):1647–1660.

Bianchi, N; E. Fornasiero and W. Soong. (2015). Selection of PM flux linkage for maximum low-speed torque rating in a PM-assisted synchronous reluctance machine. IEEE Transactions on Industry Applications, 51(5): 3600–3608.

Bonthu, S.S.R; A.K.M. Arafat and S. Choi. (2017). Comparisons of rare-earth and rare-earth-free external rotor permanent magnet assisted synchronous reluctance motors. IEEE Transactions on Industrial Electronics, 64(12): 9729–9738.

Chen, J.T. and Zhu, Z.Q. (2010). Winding configurations and optimal stator and rotor pole combination of flux switching PM brushless AC machines. IEEE Transactions on Energy Conversion, 25(2): 293–302.

Chen, M; K.T. Chau, W. Li and C. Liu. (2014). Cost-effectiveness comparison of coaxial magnetic gears with different magnet materials. IEEE Transactions on Magnetics, 50(2): 1–4.

Evans, D.J. and Zhu, Z.Q. (2015). Novel partitioned stator switched flux permanent magnet machines. IEEE Transactions on Magnetics, 51(1): 1–14.

Faiz, J; T. Asefi, M.A. Khan. (2020). Design of dual rotor axial flux permanent magnet generators with ferrite and rare-earth magnets. Electronics and Energetics, 33(4): 553–569.

Kim, K.H; H. Park, H, S. Jang, D. You and J. Choi. (2016). Comparative study of electromagnetic performance of high-speed synchronous motors with rare-earth and ferrite permanent magnets. IEEE Transactions on Magnetics, 52(7): 1–4.

Kimiabeigi, M; J.D. Widmer, R. Long, Y. Gao, J. Goss, R. Martin, T. Lisle, J.M. Soler Vizan, A. Michaelides and B. Mecrow. (2016). High-performance low-cost electric motor for electric vehicles using ferrite magnets. IEEE Transactions on Industrial Electronics, 63(1): 113–122.

Krizan, J.A. and Sudhoff, S.D. (2012). Theoretical performance boundaries for permanent magnet machines as a function of magnet type. Paper presented at IEEE Power and Energy Society General Meeting, San Diego, USA, 1–6.

Li, Y; D. Bobba and B. Sarlioglu. (2018). Design and optimization of a novel dual-rotor hybrid PM machine for traction application. IEEE Transactions on Industrial Electronics, 65(2): 1762–1771.

Obata, M; M. Shigeo, M. Sanada and Y. Inoue. (2013). High-performance PMASynRM with ferrite magnet for EV/HEV applications. Paper presented at 15th European Conference on Power Electronics and Applications (EPE2013), Lille, France, 1–9.

Xie, Z.H; D.T. Zhang, Z.F. Shang, H.G. Zhang, W.Q. Liu and M. Yue. (2019). Microstructure characteristics of 2:17 SmCo commercial magnets with different coercivities. IEEE Transactions on Magnetics, 55(7): 1–4.

Xu, H; J. Li, J. Chen, Y. Lu and M. Ge. (2021). Analysis of a hybrid permanent magnet variable-flux machine for electric vehicle tractions considering magnetizing and demagnetizing current. IEEE Transactions on Industry Applications, 57(6): 5983–5992.

Yoon, K.Y and Hwang, K.Y. (2021). Optimal design of spoke-type IPM motor allowing irreversible demagnetization to minimize PM weight. IEEE Access, 9: 65721–65729.